Thermodynamics of a binary monolayer of Ising dipolar particles. II. Effect of relative moment

Masaru Suzuki,[1,*] Ferenc Kun,[2,†] and Nobuyasu Ito[3,‡]
[1]*Department of Applied Physics, University of Tokyo, 7-3-1 Hongo, Bunkyo-ku, Tokyo 113-8656, Japan*
[2]*Department of Theoretical Physics, University of Debrecen, P.O. Box 5, H-4010 Debrecen, Hungary*
[3]*Department of Applied Physics, University of Tokyo, 7-3-1, Hongo, Bunkyo-ku, Tokyo 113-8656, Japan*
(Received 13 December 2007; revised manuscript received 21 August 2008; published 17 October 2008)

Thermodynamic behaviors of a binary monolayer of Ising dipolar particles are studied using particle dynamics simulation, varying the relative intensity between the upward and downward dipole moments. The orientational order of the solid phase changes from tetragonal to hexagonal as the moment ratio increases. On the basis of the arguments of the candidates for ground state structures, the energy of the structures are well estimated. The transition point is also determined theoretically, which is consistent with the value obtained from the simulation results. Critical condensation is also studied. While the system whose moment ratio is unity does not exhibit the gas-liquid critical condensation, the transition appears as the moment ratio changes. The local structure of the liquid phase is found to be characterized by the ground state of the tetramer. The above-mentioned results imply that the gas-liquid critical point comes close to the melting transition point as the local structure of the liquid phase becomes closer to the structure of the solid phase, and therefore, the critical condensation is vanished.

DOI: 10.1103/PhysRevE.78.041118 PACS number(s): 05.70.−a, 83.10.Pp, 75.50.Mm, 81.30.−t

I. INTRODUCTION

Polar molecules [1–14] and/or multicomponent particle systems [13,15–21] often show a rich variety of ground-state structures and thermal phases compared with single component, simple interaction particle systems. Among such systems, behaviors of the two- and three-dimensional dipolar spheres and the Stockmayer fluid have been intensively investigated recently [3–14]. Not only that the ground state of dipolar spheres have a wide variety of structures depending on particle density [10,12], it also shows critical condensation that is much different from that of a simple fluid [4,5,7,8,11]. Dipolar spheres tend to contact with head-to-tail alignment because of anisotropic pair interaction and then aggregate into elongated polymerlike chains as temperature decreases. Thus, normal gas-liquid condensation is thought to vanish from the phase diagram of this system [6,14].

Even without anisotropic interaction, a binary mixture of dipolar particles also shows interesting thermodynamic features. A monolayer of dipolar particle model in which the dipole orientation of each particle is fixed to be up or down is named the Ising dipolar particle (IDP) model [18–22], mainly whose ground-state structures [13,17,18,20] and aggregation dynamics have been investigated [19]. Regarding the thermodynamics of the IDP model, we have reported in the preceding paper that the gas-liquid critical point estimated from our simulation results is lower than the solidification temperature and the liquid phase disappears [21]. We have observed critical clusters and found that although a cluster as a whole consists of random configurations of particles, it is locally ordered to a characteristic tetragonal configuration. With an appropriate Mayer-Mayer expansion analysis considering such a local configuration, we have shown that owing to the similarity of local configurations of critical clusters with the solid order, the free energies of the liquid and solid phases differ negligibly and solidification occurs slightly ahead of condensation.

As the critical condensation of IDP is controlled by such a local characteristic structure reflecting the energy minimum of a particle configuration, the critical point may sensitively change when the relative dipole moment between two species changes from unity. Furthermore, the ground state may also change from a square lattice with alternate positions of two species. In this study the dependence of a phase diagram on the relative dipole moment is investigated.

II. MODEL AND METHOD

The model is the same as that indicated in [21], except for relative dipole moment. The system consists of N Ising dipole particles in a square box of side length L with periodic boundary condition. All the particles have the identical mass m. Each particle has a spherical elastic volume of radius R and a pointlike dipole moment at the center. The dipole moment of each particle is fixed throughout the time evolution, and it is perpendicular to the plane of motion pointing either upward or downward. The pair potential between the ith and the jth particles is

$$\Phi(r_{ij}) = \Phi^{\mathrm{pp}}(r_{ij}) + \frac{\mu_i \mu_j}{r_{ij}^3}, \tag{1}$$

with the dipole moments μ_i and μ_j of the ith and the jth particles, and the interparticle distance r_{ij}. The strength of each dipole moment is either of μ_1 or $\mu_2 \equiv -\mu_1/\mu_r$, where μ_r is the relative dipole moment. The parameter range of $1 < \mu_r$ (or $|\mu_2| < |\mu_1|$) is investigated. Hereafter, we refer to a particle with μ_1 dipole moment as a μ_1 particle, and a particle with μ_2 moment as a μ_2 particle. The ratio of the num-

*suzuki@serow.t.u-tokyo.ac.jp
†feri@dtp.atomki.hu
‡ito@ap.t.u-tokyo.ac.jp

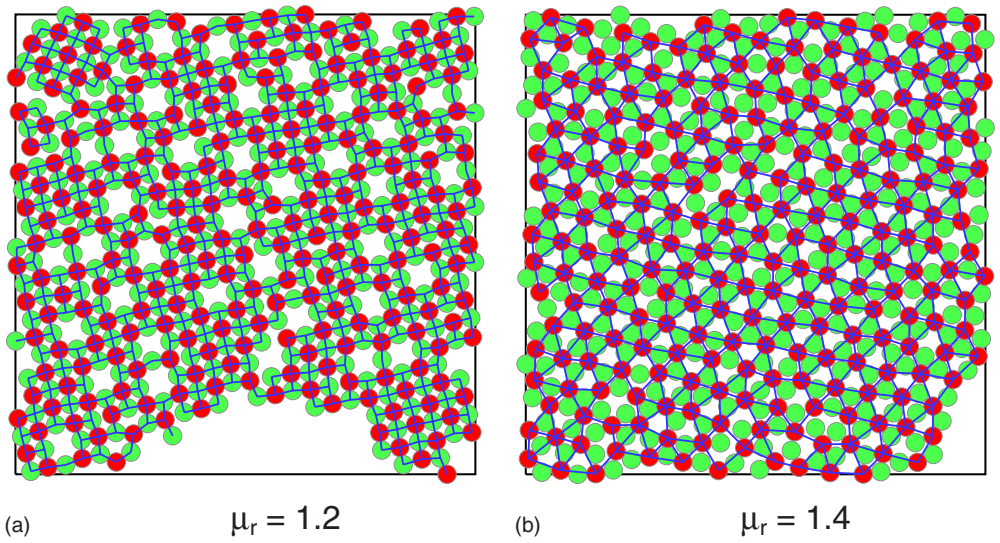

FIG. 1. (Color online) Structures of solid clusters with (a) $\mu_r=1.2$ and (b) $\mu_r=1.4$ at $T=0.032$. Red particles (or darker color) have large moments, and the other particles have small moments. Particles in (a) are positioned tetragonally, while those in (b) are positioned hexagonally.

ber of μ_1 particles (N_1) to that of μ_2 particles (N_2) is set to satisfy the neutral condition,

$$N_1\mu_1 + N_2\mu_2 = 0, \tag{2}$$

or $N_2/N_1=1/\mu_r$. Φ^{pp} denotes the core potential. For the efficiency of the particle dynamics simulation, a small overlap of particles is assumed using the Hertzian contact potential

$$\Phi^{pp}(r_{ij}) = \begin{cases} \frac{2}{5}k_{pp}(d-r_{ij})^{5/2} & (r_{ij}<d), \\ 0 & (r_{ij}>d), \end{cases} \tag{3}$$

with the elasticity constant $k_{pp}=400\sqrt{2}\mu_0^2/d^{5.5}$.

We perform a series of particle dynamics simulations under a canonical (TNV) ensemble using the method indicated in [23] (details are shown in [21]). Instead of V, hereafter we use the density defined as the coverage $\phi \equiv N\pi R^2/V$, and the Boltzmann constant is set using the binding energy of two particles as $k_B=2|\mu_1\mu_2|d^{-3}$. The cutoff distance is taken to be $R_{cf}=8d$ here, where $d(=2R)$ denotes the diameter of the particles. Most of the simulations are performed using $N=6400$ particles.

III. RESULT

To obtain the phase diagram that depends on the relative dipole moment, the structures of solid phases, the solidification temperature, and the critical point of the gas-liquid transition are investigated.

First, the growth of a solid cluster is observed for several relative dipole moments. Particles are randomly placed at the beginning of each simulation, and temperature is fixed to be $T=0.032$ for the simulation. We choose $T=0.032$ because the system constructs metastable structures at lower temperature (see [18]) and the solid structure may melt at higher temperature. Figure 1 shows the structures of the clusters for small and large relative moments. At the relative moment $\mu_r=1.2$, the structure exhibits a tetragonal order with alternate positions of the species. On the other hand, the system exhibits a hexagonal order for a larger relative moment. It is worth noting that only particles with large dipole moments (μ_1) exhibit a hexagonal order, while those with small moments (μ_2) do not. The reason for the occurrence of this phenomenon is given later.

The time evolutions of some orientational orders are studied in order to determine the structure at each relative moment. Each of the tetragonal and the hexagonal orientational orders is observed. These orientational orders are calculated as follows: For a neighboring particle pair whose relative position is $\boldsymbol{r}_{ij}\equiv(x_{ij},y_{ij})$ the orientation is defined as $\exp(\theta_{ij}\mathrm{i})=(x_{ij}+\mathrm{i}y_{ij})/r_{ij}$ with the imaginary unit i. Then the fourfold and sixfold orientational orders are determined as

$$\psi_4 = \frac{1}{N}\left|\sum_{i,j}\exp(4\mathrm{i}\theta_{ij})\right|,$$

$$\psi_6 = \frac{1}{N}\left|\sum_{i,j}\exp(6\mathrm{i}\theta_{ij})\right|. \tag{4}$$

The time evolutions of ψ_4 and ψ_6 are shown in Fig. 2. In systems with $\mu_r<1.32$, ψ_4 increases monotonically, while ψ_6 increases in $1.32\leqslant\mu_r$ systems. Therefore, the transition point between fourfold and sixfold orders is at (see Fig. 3)

$$\mu_r \simeq 1.32. \tag{5}$$

Next, the melting (solidification) temperature T_s for each μ_r is estimated by observing the time evolution of ψ_4 or ψ_6. The estimated values of T_s are summarized in Table I. Here, T_s is associated with the temperature of the tricritical point.

Finally, the critical temperature of gas-liquid condensation, T_c, is also estimated for each μ_r by the critical scaling of average cluster size. In the fluid phase, the average cluster size near the critical point should be fitted by the following scaling form using a scaling function f as

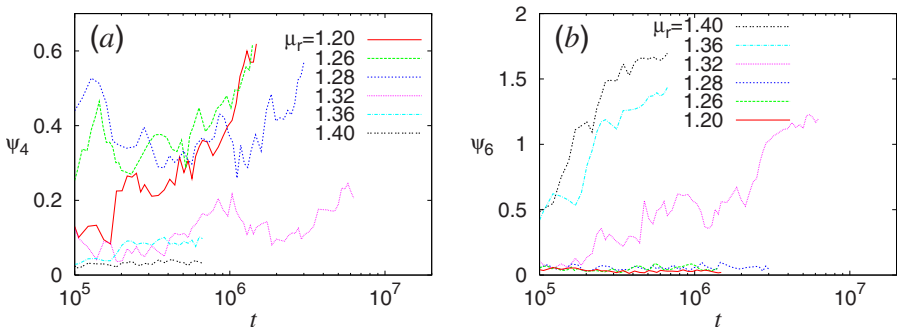

FIG. 2. (Color online) Time evolution of (a) fourfold and (b) sixfold orientational orders at $T=0.032$. The orientational order switches from tetragonal to hexagonal at approximately $\mu_r=1.32$.

$$\bar{s}/\phi \sim (T-T_c)^{-\gamma} f[(T-T_c)/(\phi_c-\phi)^a], \tag{6}$$

where (T_c,ϕ_c) is the critical point, γ and a are critical exponents, and f is a scaling function. Therefore, the average cluster size measured at each temperature and density falls onto a single curve when appropriate critical values are chosen (see [21]).

Figure 4 shows the μ_r-T phase diagram of the IDP model. The solidification temperature T_s decreases with μ_r, owing to the increasing frustration between next-nearest particles (μ_1-μ_1). After the order of the solid phase switches to hexagonal, the T_s curve exhibits another local maximum around $\mu_r \simeq 1.9$. This local maximum comes from the fact that a perfect hexatic lattice can be formed at 1:2 concentration ($\mu_r=2$) and beyond that relative dipole, a hexatic order gradually becomes unfavorable. These features are quantitatively investigated in the next section.

The critical point which was hidden under the solidification temperature becomes above T_s and a liquid phase appears as μ_r increases from 1. A snapshot of a typical gas-liquid coexistence phase is shown in Fig. 5.

IV. THEORETICAL ANALYSIS

The energy of the tetragonal lattice and that of the hexatic lattice consisting of IDPs are calculated analytically. Since the relative number of particles is $N_1/N_2=1/\mu_r$, the perfect square lattice is constructed at $\mu_r=1$, and the perfect hexatic lattice at $\mu_r=2$ (six μ_2 particles around a μ_1 particle). In an intermediate range $(1<\mu_r<2)$, both lattices should have defects of μ_1 or μ_2 particles in order to form the square or hexatic order. We perform the following analyses by assuming that those defects are located randomly.

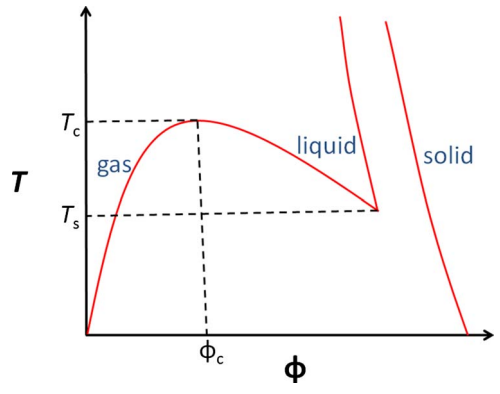

FIG. 3. (Color online) Schematic drawing of ϕ-T phase diagram for a certain μ_r. From this phase diagram, T_c and T_s are obtained (Fig. 4).

For the square lattice with the lattice constant d, the defect ratio of μ_1 particles is $p=1-1/\mu_r$. Therefore, the energy per particle is

$$\epsilon_4 = \frac{2}{(1-p)+1}\sum_i \sum_{j=-i+1}^{i} \frac{(1-p)\mu_1\mu'_{i+j}+\mu_2\mu'_{i+j+1}}{(d\sqrt{i^2+j^2})^3}$$

$$= \frac{4}{1+\mu_r}\frac{|\mu_1\mu_2|}{d^3}\sum_i \sum_{j=-i+1}^{i} \frac{(-1)^{i+j}}{(\sqrt{i^2+j^2})^3} \simeq \frac{-2.643}{1+\mu_r}\frac{|\mu_1\mu_2|}{d^3},$$

$$\mu'_k = \begin{cases} (1-p)\mu_1 & (k \bmod 2 = 0), \\ \mu_2 & (k \bmod 2 = 1). \end{cases} \tag{7}$$

The relative particle position indicated by (i,j) is explained in Fig. 6. The summation in the equation is performed within the cutoff length, i.e., $d\sqrt{i^2+j^2}<R_{cf}$. The energy per particle in a hexatic lattice is

$$\epsilon_6 = \frac{3}{1+2(1-p')}\sum_i \sum_{j=1}^{j\le i} \times \frac{\mu_1\mu'_{i+j}+(1-p')\mu_2\mu'_{i+j+1}+(1-p')\mu_2\mu'_{i+j+2}}{d^3\sqrt{i^2+j^2-ij}^3}$$

$$= \frac{9\mu_r}{4(1+\mu_r)}\frac{|\mu_1\mu_2|}{d^3}\sum_i \sum_{j=1}^{j\le i} \frac{-1+3\delta_{(i+j) \bmod 3,0}}{\sqrt{i^2+j^2-ij}^3}$$

TABLE I. The solidification (melting) temperature T_s and gas-liquid critical point (T_c,ϕ_c) at each relative moment are shown.

μ_r	T_s	T_c	ϕ_c
1	0.0585(1)	0.05790(5)	0.275(5)
1.26	0.041(1)		
1.32	0.035(1)		
1.36	0.035(1)		
1.5	0.037(1)	0.056(1)	0.31(1)
1.8	0.043(1)	0.053(1)	0.35(1)
2.0	0.042(1)	0.0525(10)	0.36(1)
2.2	0.040(1)		

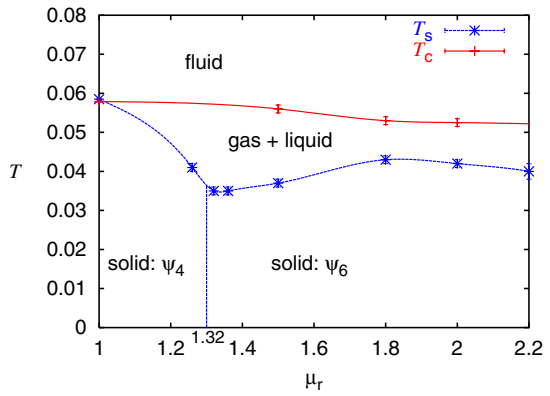

FIG. 4. (Color online) The μ_r-T phase diagram of Ising dipolar particles is shown. Curves serve as optical guides.

$$\simeq \frac{-1.743\mu_r}{(1+\mu_r)}\frac{|\mu_1\mu_2|}{d^3},$$

$$\mu_k' = \begin{cases} \mu_1 & (k \bmod 3 = 0), \\ (1-p')\mu_2 & (k \bmod 3 \neq 0), \end{cases} \tag{8}$$

where $p'=1-\mu_r/2$ is the defect ratio of μ_2 particles (for $\mu_r \leqslant 2$). The summation is within $d\sqrt{i^2+j^2-ij} < R_{cf}$.

The theoretical ϵ_4 and ϵ_6 values and the energy per particle calculated from the simulation results are shown in Fig. 7. The energy is measured at $T=0.01$ in the simulation (Table II). In the range of $\mu_r < 1.3$ where the system shows a tetragonal order, the lattice energy calculated from the simulation results agrees well with the analysis results. However, the hexatic lattice of the simulation ($1.32 < \mu_r$) has a much lower energy than that of the analysis. The transition point is predicted to be $\mu_r \simeq 1.52$, which is much higher than $\mu_r=1.32$ obtained by simulation.

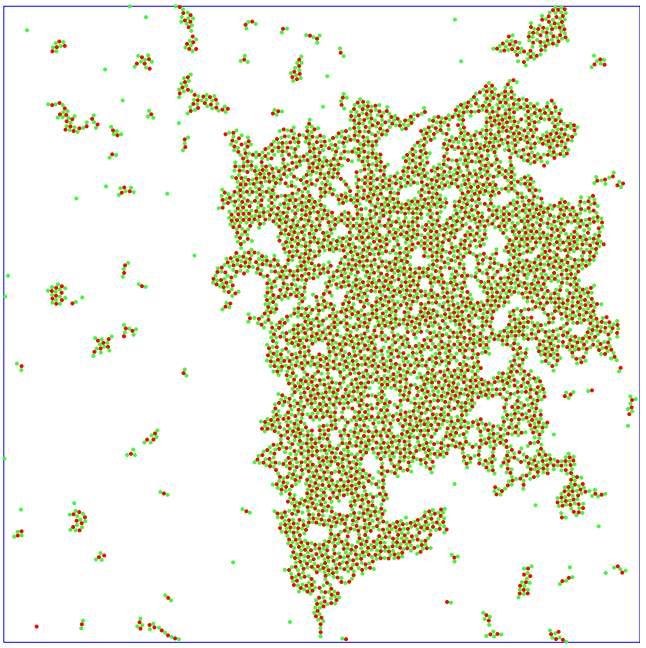

FIG. 5. (Color online) A snapshot of gas-liquid separation at $\mu_r=1.32$, $\phi=0.2$, and $T=0.05$ is shown. The largest cluster (and, maybe, larger clusters) is a liquid droplet, and the region around it consisting of monomers and small clusters corresponds to a gas phase.

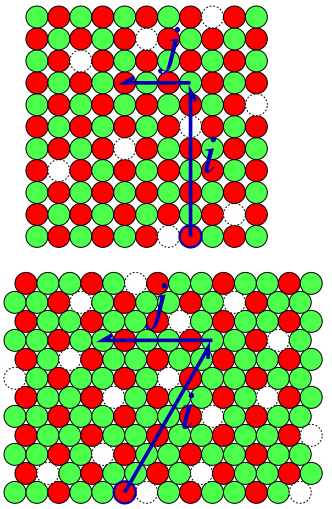

FIG. 6. (Color online) Binary square and hexatic lattice showing how the energy per particle was calculated.

Observing the image in Fig. 1(b) again, we found that μ_2 particles are loosely packed among μ_1 particles, instead of being located at the position of the perfect hexatic lattice. Such looseness should make the distance between nearest particles longer and reduce energetic frustrations between μ_2-μ_2 interactions. It seems that the hexatic lattice in the simulation has a lower energy than ϵ_6 because of this reason.

We would like to introduce another candidate of the ground-state configuration for the hexatic lattice: We assume that μ_2 particles are evenly distributed around a μ_1 particle, as illustrated in Fig. 8, instead of defects of μ_2 particles existing in a perfect hexatic configuration. The distance between neighboring μ_2-μ_2 particles is therefore changed from d to

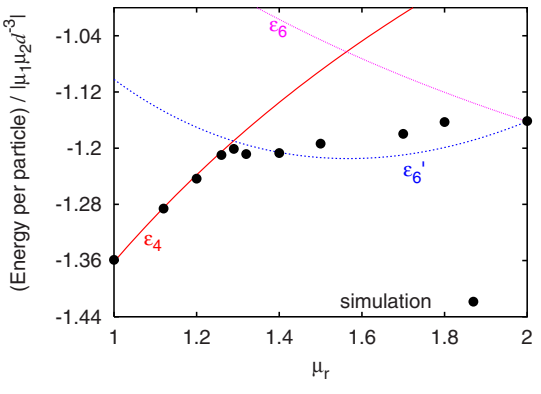

FIG. 7. (Color online) Analytical curves of energy of square lattice with μ_1 defects (ϵ_4), hexatic lattice with μ_2 defects (ϵ_6), and μ_1 hexatic lattice with loose packing μ_2 (ϵ_6') are shown and compared with the simulation results. The error bar of each plot is within the size of the circle. For the fitting of the ϵ_4 curve, the lattice constant is assumed to be $0.99d$.

TABLE II. The energy per particle in a lattice at each relative dipole is shown (measured at $T=0.01$).

μ_r	E	μ_r	E
1	−1.359(1)	1.32	−1.208(2)
1.12	−1.286(2)	1.4	−1.207(2)
1.2	−1.243(2)	1.5	−1.194(2)
1.26	−1.210(2)	1.8	−1.163(2)
1.29	−1.201(2)	2	−1.161(2)

$$r' = 2d \sin[\pi/(3\mu_r)].$$

Then the energy per particle ϵ_6 is replaced with

$$\epsilon_6' = \epsilon_6 + \frac{1}{2}\frac{2(1-p')}{3-2p'}3\left(-\frac{\mu_2^2}{d^3}(1-p') + \frac{\mu_2^2}{r'^2}\right) = \epsilon_6 + \frac{3\mu_r}{2(1+\mu_r)}\left(-\frac{1}{2} + \frac{1}{8\mu_r \sin^3[\pi/(3\mu_r)]}\right)\frac{|\mu_1\mu_2|}{d^3}, \tag{9}$$

considering that the ratio of the number of μ_2 particles to the total number of the particles is $N_2/N=2(1-p')/(3-2p')$. The ϵ_6' curve as a function of μ_r is shown in Fig. 7. While there still remains a small difference from the simulation results, it is much improved compared to the previous ϵ_6 curve. Moreover, the transition point obtained from ϵ_4 and ϵ_6' is estimated to be $\mu_r=1.29$. This value is much closer to the value from the simulation result.

Next, the features of critical condensation and the relationship between T_c and T_s are also investigated. As in the case of $\mu_r=1$ [21], the particles in the fluid phase near the critical condensation may locally form a typical configuration that can be well characterized by the ground-state configuration of the small number of particles. To clarify this point, the local configuration of critical clusters is observed: The average distance between neighboring μ_1-μ_1 particles (denoted as d_{++}) and that of μ_2-μ_2 particles (d_{--}) in the critical region are measured (Fig. 10). The d_{++} and d_{--} values differ as μ_r increases.

On the other hand, the ground-state configuration of a four-particle cluster with two-by-two particles is rhombic as illustrated in Fig. 9, and the energy of such a configuration is

$$\epsilon_t = \frac{1}{2}\left(\frac{4\mu_1\mu_2}{d'^3} + \frac{\mu_1^2}{A^3} + \frac{\mu_2^2}{B^3}\right) = \frac{\mu_1\mu_2}{2}\left(\frac{4}{d'^3} - \frac{1}{\mu_r A^3} - \frac{\mu_r}{B^3}\right) \tag{10}$$

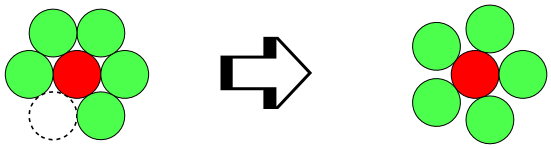

FIG. 8. (Color online) As a model assumption, configurations of neighboring μ_2 particles are changed such that the μ_2 particles are evenly distributed around a μ_1 particle (showing the case for $\mu_r=5/3$).

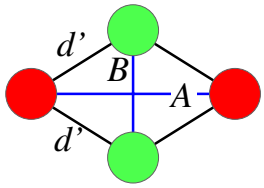

FIG. 9. (Color online) Ground-state configuration of a tetramer at $\mu_r \neq 1$.

$$(A^2 + B^2 = 4d'^2),$$

where d', A, and B are the distances between μ_1-μ_2, μ_1-μ_1, and μ_2-μ_2 particles, respectively. By calculating the local minimum condition, $\partial\epsilon_t/\partial A=0$, under the constant d', the interparticle distances of the ground state are obtained as

$$A = \frac{2d'}{\sqrt{1+\mu_r^{4/5}}}, \quad B = 2d'\sqrt{\frac{\mu_r^{4/5}}{1+\mu_r^{4/5}}}. \tag{11}$$

As shown in Fig. 10, measured d_{++} and d_{--} show good agreement with the theoretical curves A and B. Thus, the typical local configuration of critical clusters is well characterized by the ground-state configuration of a tetramer, such as that in Fig. 9. Furthermore, the ground-state energy of a tetramer in Eq. (10) is

$$\epsilon_t = \frac{\mu_1\mu_2}{d'^3}\left(4 - \frac{(1+\mu_t^{4/5})^{5/2}}{8\mu_r}\right), \tag{12}$$

which depends much less on μ_r as compared with the energy of the solid phase, ϵ_4 in Eq. (7).

As discussed here, the typical configuration and energy of critical clusters differ from those of a solid lattice as μ_r increases from 1, whereas they are very similar to the long-range order of a solid phase at $\mu_r=1$. Consequently, T_c deviates from T_s and a liquid phase appears (see Fig. 4).

V. SUMMARY AND DISCUSSION

Thermodynamics of an IDP model depending on μ_r was investigated by particle dynamics simulation. A transition of

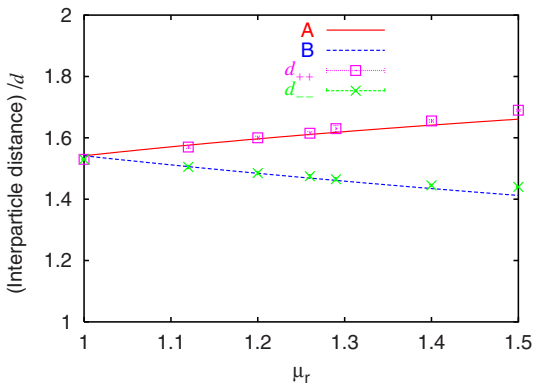

FIG. 10. (Color online) The distance between neighboring particles of critical clusters and the particle configuration of a ground-state rhombic tetramer are compared. The curves A and B are drawn by setting $d'=1.09d$.

the orientational order of a ground state from the tetragonal lattice to the hexagonal lattice of μ_1 particles with loosely packed μ_2 particles was observed at $\mu_r=1.32$. This transition was well reproduced theoretically by comparing the energy of a square lattice with alternate positions of two species and that of a μ_1 hexagonal lattice with loosely packed μ_2 particles.

The critical condensation of the $\mu_r=1$ case has been discussed in [21]: In the critical temperature region, clusters locally exhibit many tetragonal configurations of particles, and owing to the similarity of the configurations with the order of the solid phase, the values of T_c and T_s are very close, and the critical condensation disappears since $T_s>T_c$ as illustrated in Fig. 11. On the other hand, the typical local configuration of critical clusters that varies in the case of $1<\mu_r$ is well characterized by the energy minimum configuration of a four-particle cluster (rhombic configuration). As the configuration becomes less similar to the solid order, T_c deviates from T_s and a liquid phase appears.

It was clarified that in a binary mixture of particles such as the IDP model, phase transitions sensitively depend on the energy balance between two species. Therefore, other variations in a parameter, for example, changes in the relative condensation of two species, may also change the thermodynamic phases. Although this study is restricted within neutral conditions, analytical calculations of lattice energies (ϵ_4, ϵ_6, and ϵ_6') in Eqs. (7)–(9) are also applicable to non-neutral conditions, by setting $p=1-N_1/N_2$ and $p'=1-N_2/(2N_1)$. In the 1:1 concentration, a μ_1 particle in a lattice used for ϵ_6' calculation has three μ_2 neighbors (and vice versa). This structure is very similar to the honeycomblike lattice reported in [17,18,20]. Here, an interesting prediction arises:

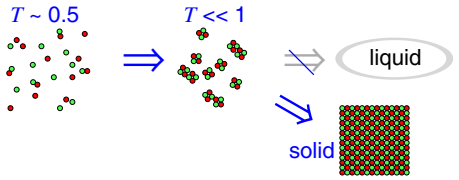

FIG. 11. (Color online) The transition of IDP at $\mu_r=1$ is schematically illustrated.

The solid phase with a loose packing hexatic order continuously changes to the honeycomblike lattice, as the relative concentration varies to be $N_1/N_2\to 1$. This is expected to be verified by further investigation.

The analyses presented in this paper can be applicable to other complex fluids with an anisotropic interaction and/or multicomponent mixture where the energy sensitively changes depending on the microscopic particle orientation or configuration. As we have pointed out, such a system forms a typical local configuration which is similar to the ground-state configuration even in the fluid phase at a relatively high temperature. And that configuration plays a dominant role in phase transitions. Thus, it is necessary to determine the type of structure locally formed to understand the characteristics of transitions in such systems.

ACKNOWLEDGMENTS

The authors thank T. Shimada and H. Watanabe for fruitful discussions. The present study was partially supported by KAKENHI (Contract No. 19340110), and F.K. was supported by the research grant OTKA T049209.

[1] H. Sun and R. O. Watts, J. Chem. Phys. **96**, 1810 (1992).
[2] A. S. Clarke and G. N. Patey, J. Chem. Phys. **100**, 2213 (1994).
[3] P. I. C. Teixeira, J. M. Tavares, and M. M. Telo da Gama, J. Phys.: Condens. Matter **12**, R411 (2000).
[4] M. J. Stevens and G. S. Grest, Phys. Rev. E **51**, 5962 (1995).
[5] J. M. Tavares, J. J. Weis, and M. M. Telo da Gama, Phys. Rev. E **73**, 041507 (2006).
[6] J. M. Tavares, M. M. Telo da Gama, and M. A. Osipov, Phys. Rev. E **56**, R6252 (1997).
[7] T. Tlusty and S. A. Safran, Science **290**, 1328 (2000).
[8] P. J. Camp, J. C. Shelley, and G. N. Patey, Phys. Rev. Lett. **84**, 115 (2000).
[9] J. C. Shelley, G. N. Patey, D. Levesque, and J. J. Weis, Phys. Rev. E **59**, 3065 (1999).
[10] J. Stambaugh, D. P. Lathrop, E. Ott, and W. Losert, Phys. Rev. E **68**, 026207 (2003).
[11] D. L. Blair and A. Kudrolli, Phys. Rev. E **67**, 021302 (2003).
[12] J. J. Weis, Mol. Phys. **100**, 579 (2002).
[13] W. D. Ristenpart, I. A. Aksay, and D. A. Saville, Phys. Rev. Lett. **90**, 128303 (2003).
[14] Y. Levin, Phys. Rev. Lett. **83**, 1159 (1999).
[15] I. Szalai and S. Dietrich, Mol. Phys. **103**, 2873 (2005).
[16] A.-P. Hynninen and A. Z. Panagiotopoulos, Phys. Rev. Lett. **98**, 198301 (2007).
[17] I. Varga, H. Yamada, F. Kun, H.-G. Matuttis, and N. Ito, Phys. Rev. E **71**, 051405 (2005).
[18] I. Varga, F. Kun, and K. F. Pál, Phys. Rev. E **69**, 030501(R) (2004).
[19] N. Yoshioka, I. Varga, F. Kun, S. Yukawa, and N. Ito, Phys. Rev. E **72**, 061403 (2005).
[20] I. Varga and F. Kun, Philos. Mag. **86**, 2011 (2006).
[21] M. Suzuki, F. Kun, S. Yukawa, and N. Ito, Phys. Rev. E **76**, 051116 (2007).
[22] I. Varga, N. Yoshioka, F. Kun, S. Gang, and N. Ito, J. Stat. Mech.: Theory Exp. (2007) P09015.
[23] D. J. Evans and G. P. Morriss, Phys. Lett. **98A**, 433 (1983).